Loughlin et al., http://www.jcb.org/cgi/content/full/jcb.201006076/DC1



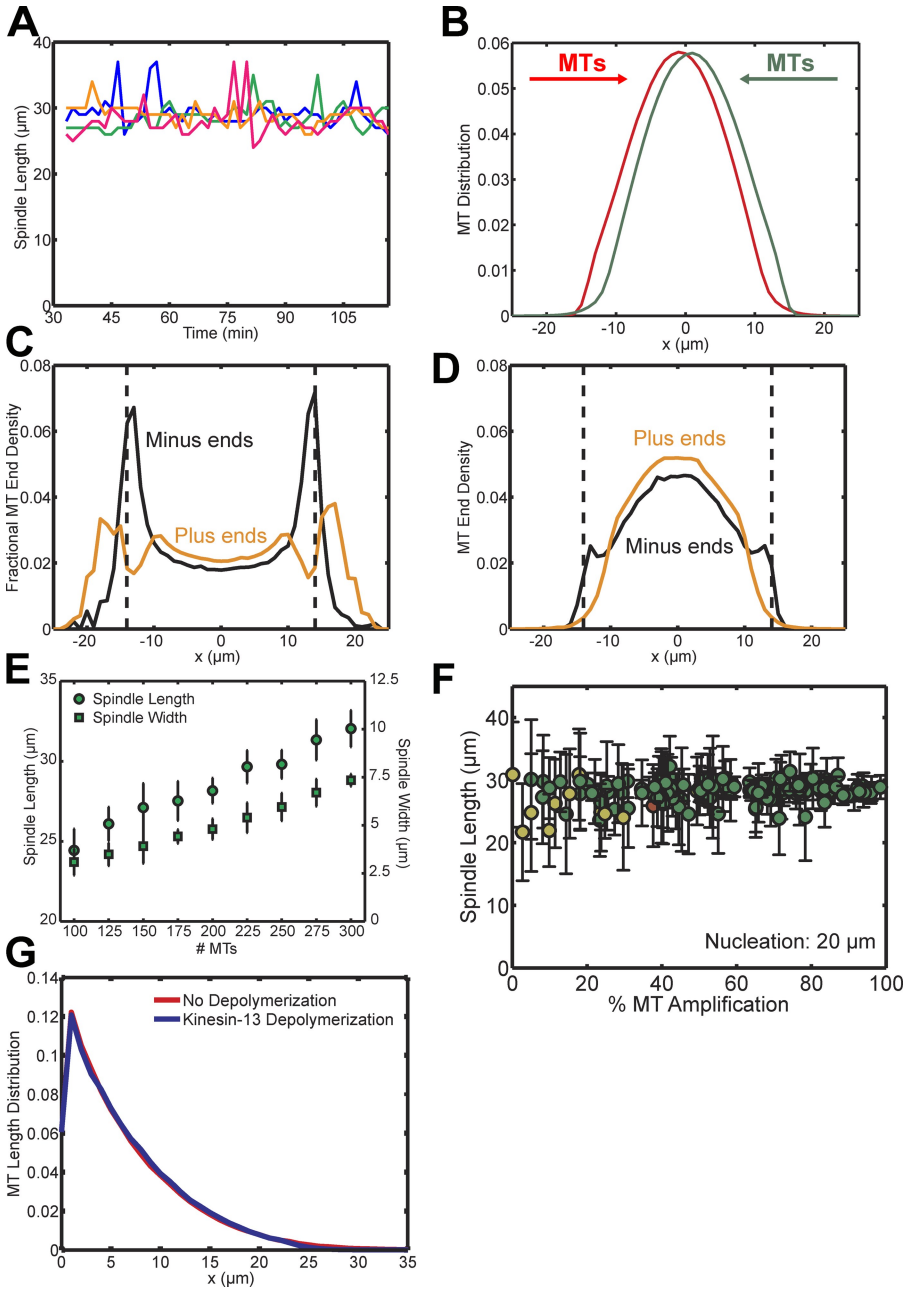


Figure S1. **Steady-state spindles replicate experimental measurements.** (A) Average spindle length from four different simulations, indicating that spindles reached a steady state. (B) Oriented MT density distribution (MTs oriented to the right in red, to the left in green) represents a bipolar structure with minus ends at the extremity and antiparallel MT overlap in the midzone (95 simulations). (C) Fractional minus (black) and plus (orange) end densities from steady-state spindles. Dashed lines represent the average pole position. A very high percentage of the MT density at the pole consists of minus ends, whereas most astral MT density consists of plus ends (95 simulations). (D) Minus (black) and plus (orange) end densities from steady-state spindles. Dashed lines represent the average pole position. Minus-end density displayed an additional peak at the spindle pole,whereas plus ends closely reflected the MT density (B; 95 simulations). (E) Spindle length (mean ± SEM; circles) and width (mean ± SEM; squares) were proportional to the number of MTs in the spindle (94 simulations). (F) When the percentage of chromatin-mediated MT nucleation was varied in the control simulation, where the two nucleation pathways significantly spatially overlapped, the bipolarity of MT structures was unaffected (green and yellow). Spindle length (mean ± SD) also did not significantly vary with the nucleation pathway (131 simulations). (G) MT length distribution in MT structures with (blue) and without (red) kinesin-13 depolymerization demonstrate the minute effect of the pole formation mechanism on global MT dynamics (100, 72 simulations).

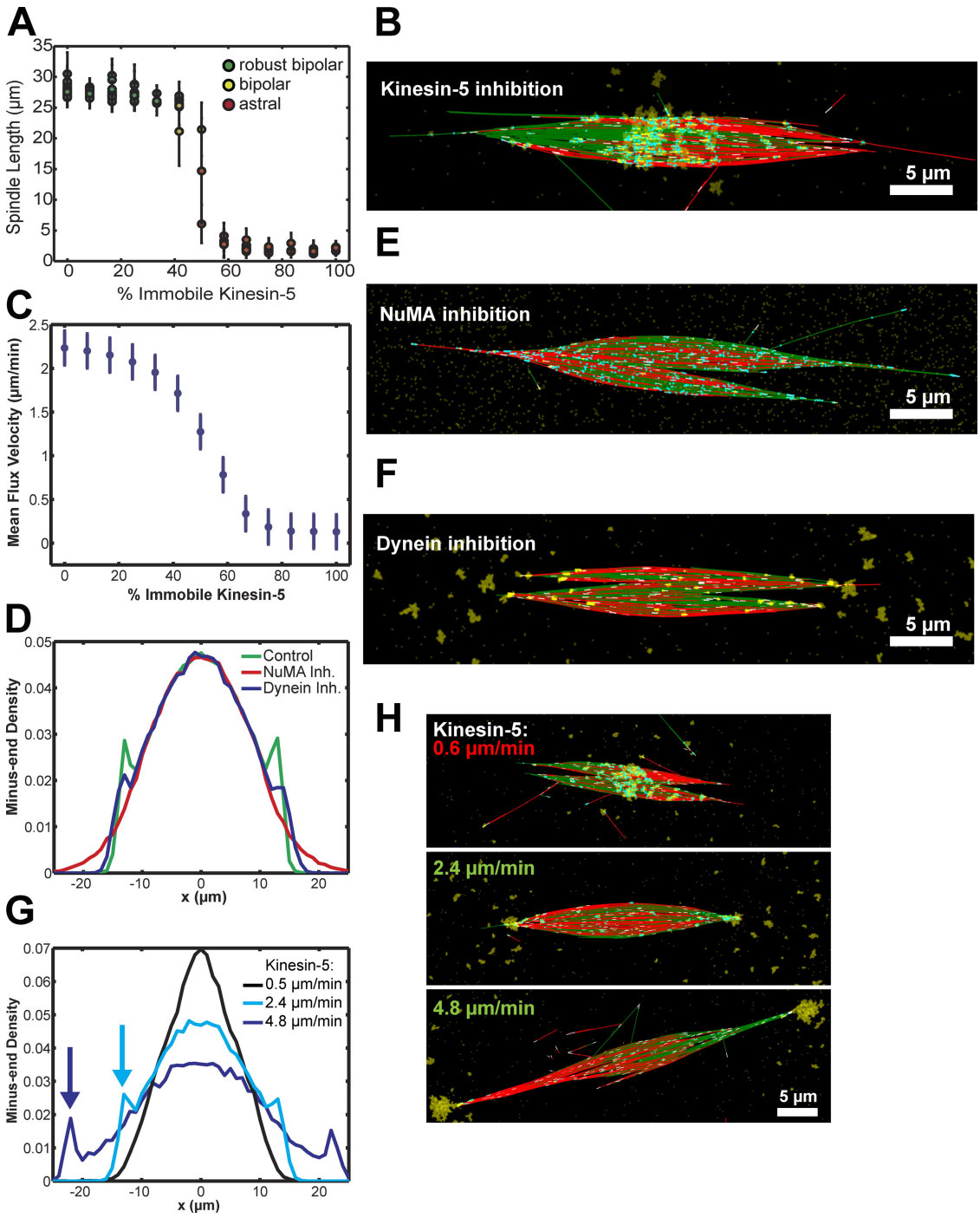


Figure S2. **Simulated spindles replicate experimental inhibition phenotypes.** (A) Spindle length (mean ± SD) decreased with increasing percentage of immobile kinesin-5 until a threshold value. Color indicates bipolar index (114 simulations). (B) Representative astral MT structure with kinesin-5 inhibition. MTs are oriented with plus ends outward, and NuMA accumulates at a single pole in the center of the structure. The bundling interaction prevents radial aster formation. (C) Mean flux velocity in μm/min (mean ± SE) of spindles decreased nonlinearly with increasing percentage of immobile kinesin-5 (114 simulations). (D) Normalized minus-end density in control (green), NuMA-inhibited (red), and dynein-inhibited (blue) MT structures. Dynein inhibition decreased the efficiency of pole formation, whereas inhibiting NuMA oligomerization abolished it (72, 20, 20 simulations). (E) Representative MT structure with NuMA inhibition. Without the ability to oligomerize, NuMA does not significantly accumulate on MTs. (F) Representative MT structure with dynein inhibition. Small NuMA oligomers localize to distal MT minus-ends through direct MT binding and transport via MT flux. (G) Spindle pole formation (cyan and blue arrows), as indicated by a peak in minus-end density, occurred over a range of kinesin-5 velocities. At very low velocities (black), astral structures formed with a single central cluster of minus ends (mean from 4, 6, and 7 simulations for each kinesin-5 velocity). (H) Range of steady-state MT structures obtained with different kinesin-5 velocities. Text color designates bipolarity index. Bars, 5 μm.

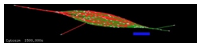

Video 1. **Kinesin-5 generates fluxing MT arrays but fails to focus poles.** Simulations containing MTs, a cross-linking force, and kinesin-5 generated MT arrays (red and green, color indicates orientation) in which MTs slid outward. However, minus ends were dispersed throughout the structure, and focused spindle poles did not form. Bar (blue), 5 µm.

Video 2. **Kinesin-5 remains stationary in fluxing MT arrays.** In simulations containing MTs, a cross-linking force, and kinesin-5 (orange), kinesin-5 remained stationary while MTs fluxed. Kinesin-5 traveled to the plus end of each bound MT at the same rate of MT sliding, thus maintaining a constant position while MTs slid relative to each other. Bar (blue), 5 µm.

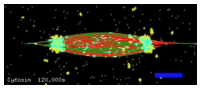

Video 3. **Cross-linking and depolymerization activities delivered to MT minus-ends generate robust spindles.** Bipolar, fluxing spindles with focused poles formed in simulations containing MTs (red and green), a cross-linking force, kinesin-5, minus-end delivery of oligomeric NuMA (yellow and cyan), and kinesin-13 MT depolymerization activity in the vicinity of NuMA. A high density of minus ends (white) can be observed at each spindle pole. Bar (blue), 5 µm.

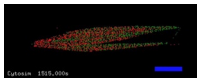

Video 4. **Tubulin speckles demonstrate antiparallel MT sliding and flux.** The same simulation as in Video 3 is shown, but MTs are displayed as randomly incorporated tubulin speckles, as is observed experimentally when low amounts of fluorescently labeled tubulin are incorporated into the spindle. MTs oriented with plus ends to the right (green) can be seen to flux to the left, whereas MTs oriented to the left (red) flux to the right. Bar (blue), 5 µm.

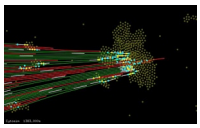

Video 5. **Kinesin-13 pole formation generates a stable equilibrium pole position.** Magnified video of a simulated spindle pole. MT minus-ends (white) slide to the spindle pole, where they are eventually depolymerized at the same rate at which MTs slide poleward. Small oligomers of NuMA (yellow and cyan) are constantly delivered to the pole. The spindle pole position oscillates about a mean value with variation in the number of MTs arriving at the pole and in the amount of pole-localized NuMA. Bar (blue), 1 µm.

Table S1. **Comparison of measured and simulated measurements**

| **Spindle** | **% MTs to midzone at pole** | **% MTs to pole at midzone** |
|---|---|---|
| *X. laevis* | 90 (Heald et al., 1997) | 50 (Heald et al., 1997) |
| *X. laevis* – dynein inh. | 95 (Heald et al., 1997) | 50 (Heald et al., 1997) |
| Simulation | 82 ± 5 (SE) | 50 ± 1 (SE) |
| Simulation – dynein inh. | 84 ± 4 (SE) | 50 ± 1 (SE) |
| **Spindle** | **Length (µm)** | **Flux rate (µm/min)** |
| *X. laevis* | 35 (Brown et al., 2007) | 1.95 ± 0.68 (SD; G. Yang et al., 2007)<br>2.75 ± 0.75 µm/min (SD) in bead spindles (Yang et al., 2008) |
| *X. tropicalis* | 22 (Brown et al., 2007) | 2.25 ± 0.25 (SD; Brown et al., 2007) |
| Simulation | 28.27 ± 0.87 (SD) | 2.24 ± 0.01 (SE) |

| **Reference** | **Mean length (µm)** | **Distribution** | **Method** |
|---|---|---|---|
| Simulation | 6.51 ± 0.19 µm (SE) | Truncated exponential | Simulated spindle |
| Needleman et al., 2010 | – | Exponential | Speckle stability in spindles |
| Athale et al., 2008 | 4.23 µm | – | Centrosomes |
| G. Yang et al., 2007 | 20.11 ± 12.23 µm (SD) | Truncated normal | Correlation of speckles |
| Burbank et al., 2006 | 14 µm | – | Speckle flux in spindles |
| Verde et al., 1992 | 3.2 ± 0.8 µm | Exponential | Centrosomes |